A Koopman operator approach for the pitch stabilization of a hydrofoil in an unsteady flow field

Colin Rodwell Jake Buzhardt Phanindra Tallapragada

***Abstract*— The control of swimming robots presents several challenges, in large part due to the complex fluid-structure interaction. Low fidelity simplified formulas for drag and lift force lead to control amenable models, but do not capture key physics that can play an especially important role in the swimming of small-scale robots with limited actuation. Higher fidelity models of the fluid-structure interaction lead to nonlinear high dimensional control systems for which solution methods are not obvious. We propose the use of the Koopman operator in developing a linear representation for both the complex fluid structure interaction as well as actuation effects. As a test case for this framework we address the problem of stabilizing the pitching oscillations of a hydrofoil that is hinged in a simulated unsteady free stream flow. The actuator for the hydrofoil is an internal reaction wheel which presents an integral saturation constraint. Using the Koopman operator, the lifted control system is used to formulate a constrained optimal control problem which we solve using model predictive control. The framework proposed in this paper can potentially be extended to design a combination of data-driven and physics-based control algorithms for swimming robots.**

I. Introduction

The locomotion of fish and other aquatic swimmers has many desirable characteristics such as energy efficiency, agility, and stealth [1], which have inspired the design of many biomimetic robots. Designs for fish-like robots imitating the motion of tails and fins beginning with at least [2] . In all such designs, the small size of the fish-like robots and the resulting constraints on actuation and power require that for efficient and agile motion, the robots harness the fluid-structure interaction [3]. The control of such robots therefore requires modeling of the fluid-structure interaction that determines the forces and moments on a robot. Low fidelity models using simplified formulas for drag and lift forces are amenable for control, but do not capture key physics that can especially play an important role in the swimming of small-scale robots with limited actuation. Higher fidelity models of the fluid-structure interaction lead to high dimensional nonlinear control systems for which solution methods are not obvious. To overcome the challenges of the complex physics, a more suitable representation of the governing model that is also simultaneously amenable to standard control systems tools is desirable.

This approach has proven fruitful to obtain reduced order linear models and identification of dominant modes of in fluid flows, see for example [4], [5]. More recent progress has been made on the extending the Koopman operator methods to control systems, see for example [6]–[8] and for robotics specifically [9]–[11]. In particular, [6] proposes an approach to formulate a high dimensional linear control system that is amenable to model predictive control (MPC). This can enable the formulation of high-dimensional constrained linear optimal control problems, which is well suited for the problem of controlling the motion of swimming robots as it generates a convenient linear representation for both the complex governing dynamics and control input while also allowing state constraints to avoid over-extension or rotor saturation.

This paper considers the problem of stabilizing the pitching motion of a hydrofoil which is hinged in a simulated unsteady free stream flow, where the direction and the speed of the free stream flow varies in time. The actuation is a torque generated by a reaction wheel inside the hydrofoil. Reaction wheels have been shown to enable both propulsion [12], [13] and fast turning motion and path tracking with small errors in swimming robots [14]–[16]. Reaction wheels as actuators have the usual constraint of a maximum torque, but additionally have a constraint on the integral of the torque applied: when the spin angular velocity of the reaction wheel driven by a motor reaches a maximum, the torque that it applies drops to zero.

While the reaction wheel driven stabilization of a hydrofoil is novel, extensive work exists on using linear models for the stability of airfoils. Perhaps the simplest implementation is linearizing the rigid body equations of motion about the point to be stabilized by calculating "stability derivatives", and using linear control algorithms [17]. However, this approach suffers approximation error that increases rapidly with deviation from the linearization point [17], and does not account for the unsteady fluid state, which itself is a function of both current and past rigid body state. In flutter problems, unsteady aerodynamic effects are accounted for by extending this linearized state-space with aerodynamic states approximated by Rational Function Approximators [18], but this approach is only applied on specific mode shapes, which may not be present in more general problems. Low dimensional nonlinear models such as the Goman-Khrabrov model [19] are also common in aerospace applications, which provides an analytical approximation of the dynamics of the flow stagnation point of the unsteady separated flow over an airfoil. From there, the lift and drag acting on the body can be approximated or optimized for [20]–[22] based on the flow separation and angle of attack. While this model

This work was supported by grant 2021612 from the National Science Foundation and grant 13204704 from the Office of Naval Research.

Colin Rodwell, Jake Buzhardt and Phanindra Tallapragada are with the Department of Mechanical Engineering, Clemson University, Clemson, SC, 29631, USA. {crodwel@g.clemson.edu, jbuzhar@g.clemson.edu, ptallap@clemson.edu}.

has the advantage of being based on known physics, it is limited to particular applications and typically still requires the estimation of several unknown model parameters.

Recent progress on data-driven methods to model dynamical systems using the Koopman operator can be valuable for problem of stabilizing the pitching motion of a hydrofoil without relying on linearization or estimation of parameters in a nonlinear model. The Koopman operator-based method used in this paper provides a systematic means of obtaining a high-dimensional linear model accounting for unsteady aerodynamics by seamless integration of pressure data from the hydrofoil surface into the state-space model. It can be generalized to more complex physical settings such as interacting hydrofoils. Essentially, the Koopman operator acts linearly on a "lifted" space of functions that is associated with the observables of the dynamical system, see for instance [23]–[25] for a review. Considering the evolution of observable functions of the states rather than the states themselves leads to a linear but infinite dimensional dynamical system, which in practice can be projected onto a finite, but high-dimensional space. The Koopman operator MPC framework can incorporate constraints (such as the saturation of the actuation integral) by extending the basis functions of the lifted linear space to include states of the reaction wheel or more generally the dynamics of the actuator. The data-driven framework requires trajectory data from the system that covers a large part of the state space, which can be difficult to obtain experimentally without prior knowledge of the dynamics and the effect of the feedback control. Simulations are a first step to easily collect data for such methods and creating control systems that can then be improved via experiments [26].

The problem of stabilization of the pitching of a hydrofoil is motivated by several problems in swimming robots: from steering a robot in an upstream current, to attitude control for a robotic platform that is stationary. Similar problems have a rich history in aerospace engineering, where lift and drag forces on an airfoil are sought to be controlled in an unsteady flow. We expect that the work in this paper will have relevance to other control problems for flying and swimming robots.

II. Modeling

We consider a hydrofoil modeled as a NACA 0018 symmetrical airfoil pinned at its leading edge in a free-stream with speed U_0, directed at an angle $\phi(t)$ where $\phi = 0$ corresponds to horizontal flow from left to right as shown in Fig 1. The foil is actuated by an inertial reaction wheel with moment of inertia I_r.

A. Numerical simulation of fluid-structure interaction

Calculations for the flow over airfoils and hydrofoils is an old and well-studied problem. A collection of inviscid flow solvers known as panel methods [27], [28] continue to be a preferred simulation tool for high Reynolds number fluid interaction problems. In these methods, boundary surfaces are decomposed into discrete *panels* with source and vortex

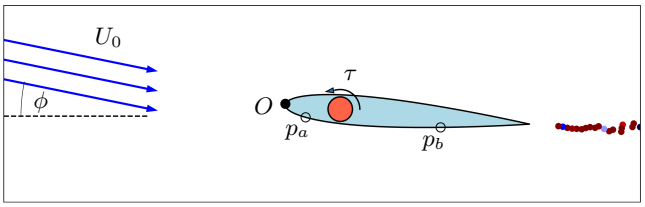

Fig. 1: Schematic of a hydrofoil pinned at its leading edge (point O) in an unsteady free stream flow with speed $U_0(t)$ at an angle $\phi(t)$. The foil has an internal reaction wheel which can exert a torque τ on the foil. Also shown are two points at which pressures p_a and p_b are measured. A line of point vortices is shed at the trailing edge of the foil.

distributions on each panel such that fluid flow does not pass through the surface. While the lack of viscous effects can reduce simulation fidelity compared to modern meshed Navier-Stokes solvers, panel methods have lower computational cost and easily incorporate body movement due to the lack of meshing. We adopt the vortex panel method for the numerical simulations of the fluid-structure interaction.

In a vortex panel method, each of the M panels has a source distribution of strength σ_i, which varies between panels, and a vortex distribution of strength γ which is constant over the body. The Neumann boundary condition is used; it stipulates that no flow passes through a panel midpoint, or $\langle u_i, \eta_i \rangle = 0 \; \forall \; i \in \{1, \ldots, M\}$, where u_i is the flow velocity vector at the center of panel i relative to the body, and η_i is the surface normal unit vector at the same control point. The Kutta condition enforces the condition that static pressures p is continuous at two panel points adjacent to the tail, i.e., $p_1 = p_M$. To preserve circulation, vortex shedding occurs at the trailing edge by calculating the change in circulation about the body at every time step and and applying an opposite circulation to a *wake panel* at the trailing edge, which is then shed as a point vortex of equal circulation at its center. The structure of the system allows γ to be solved independently, and because the flow velocity due to a specific source or vortex panel is linear in its unknown strength, the N unknown σ_i values can be found by solving the linear system of N equations arising from the Neumann boundary condition. With γ and the σ_i found, the flow field is fully determined, and the pressure distribution around the body can be computed from the unsteady Bernoulli equation. From the pressures, the resultant torque acting on the body can be computed. Then the angular acceleration of the body is found as the total torque (including the rotor torque) acting on the foil, and is equal to $I_r\dot{\omega}$. This can be integrated to determine the body dynamics. A snapshot from the simulation of the vortex wake due to a time-varying free stream speed $U_0(t)$ and angle $\phi(t)$ is shown in Fig 2.

III. Koopman Lifting and MPC

Koopman-based methods for model predictive control have received significant attention in recent years (see, for

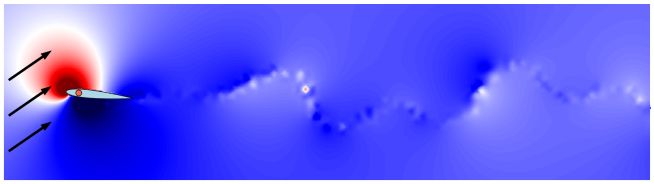

Fig. 2: A snapshot from a simulation of the interaction of the pinned hydrofoil in an unsteady flow using the panel method. The magnitude of fluid velocity is shown, with the color map defined between dark blue at $|v| = 0.5$ and dark red at $|v| = 2$. The time varying velocity free stream velocity produces a non periodic vortex wake.

example [6], [29], [30]), as MPC provides an efficient means of solving the optimal control problem that can handle constraints and be implemented online in a feedback manner. In this paper, we take the approach of [6], which modifies the extended dynamic mode decomposition (EDMD) algorithm [31] to account for the effects of actuation on the system dynamics. More recent works [29], [30] have shown that a similar data-driven approach can be used to obtain a continuous time, bilinear representation of the system based on the Koopman generator, which can then be implemented for control in a receding horizon manner. While this method appears to be more data efficient [29], the resulting system is bilinear and thus the optimal control problem must be solved either by using nonlinear optimization methods [29], [30] or by quantizing the control input and reducing the problem to selecting a control from a pre-defined set on each step, as suggested by [29], [32]. In addition, these methods also require that data on the derivatives of the states either be measured or computed by finite differencing, while the discrete-time approach only requires information about the states. For these reasons, we opt for the alternative approach of [6], which gives a linear representation of the system and thus a convex formulation of the optimal control problem.

The following subsections briefly outline the approach, beginning with a description of the EDMD method for uncontrolled systems in Sec. III-A and the extension to actuated systems in Sec. III-B.

A. Koopman operator for uncontrolled systems

The Koopman operator is an infinite dimensional linear operator which propagates observable functions of the states forward in time under the dynamics of the system. That is, for the dynamical system

$$x_{t+1} = F(x_t) \tag{1}$$

where $x_t \in \mathbb{X} \subset \mathbb{R}^n$ and $F : \mathbb{X} \mapsto \mathbb{X}$ the action of the Koopman operator $\mathcal{K} : \mathcal{L}^\infty(\mathbb{X}) \mapsto \mathcal{L}^\infty(\mathbb{X})$ on an observable function $g : \mathbb{X} \mapsto \mathbb{R}$ is given as follows.

$$\mathcal{K}g(x_t) = (g \circ F)(x_t) = g(x_{t+1}) \tag{2}$$

To approximate the infinite dimensional operator $\mathcal{K}$, we take the approach of extended dynamic mode decomposition (EDMD) by projecting the observable function g onto the space spanned by a set, $\mathbb{D}$, of dictionary functions.

$$\mathbb{D} = \{\psi_1, \psi_2, \ldots, \psi_k\} \tag{3}$$

That is, we make the approximation

$$\mathcal{K}g(x_t) \approx \mathcal{K}(c^\intercal \Psi)(x_t) \approx c^\intercal K^\intercal \Psi(x_t) \tag{4}$$

where $\Psi : \mathbb{X} \mapsto \mathbb{R}^k$ is a column-vector valued function where the elements are given by $[\Psi(x)]_i = \psi_i(x)$, $c \in \mathbb{R}^k$ is a column vector of coefficients, and $K \in \mathbb{R}^{k \times k}$ is the projection of Koopman operator onto the space of functions spanned by the dictionary $\mathbb{D}$.

To compute the matrix approximation K of the Koopman operator from data, we gather and store data in the form of snapshot matrices

$$X = \begin{bmatrix} x_1 & , & \cdots & , & x_m \end{bmatrix} \tag{5}$$

$$Y = \begin{bmatrix} y_1 & , & \cdots & , & y_m \end{bmatrix} \tag{6}$$

where the matrices X and Y contain m state observations on the columns and where $y_i = F(x_i)$ for $i = 1, \ldots, m$. We then lift the measurement data by evaluating the dictionary functions at each measurment to obtain the lifted data matrices $\Psi_X, \Psi_Y \in \mathbb{R}^{k \times m}$ as follows.

$$\Psi_X = \begin{bmatrix} \Psi(x_1) & , & \cdots & , & \Psi(x_m) \end{bmatrix} \tag{7}$$

$$\Psi_Y = \begin{bmatrix} \Psi(y_1) & , & \cdots & , & \Psi(y_m) \end{bmatrix} \tag{8}$$

Then, following from Eqs. 2 and 4, we have

$$\Psi_Y = K^\intercal \Psi_X. \tag{9}$$

With this, K can be computed by the following least-squares minimization

$$\min_K \|\Psi_Y \Psi_X^\intercal - K^\intercal \Psi_X \Psi_X^\intercal\|_2^2 \tag{10}$$

where the least squares problem has been written in normal form so that the minimization only depends on the number of dictionary functions used in the projection, not on the number of measurements.

B. Controlled systems

For a control system of the form

$$x_{t+1} = F_u(x_t, u_t) \tag{11}$$

where $u_t \in \mathbb{U} \subset \mathbb{R}^p$ is the control input and $F_u : \mathbb{X} \times \mathbb{U} \mapsto \mathbb{X}$, we take a similar approach to obtain a linear representation of the system in a lifted space. That is, we seek a linear approximation of the form

$$\Psi(x_{t+1}) = A\Psi(x_t) + Bu_t \tag{12}$$

where $A \in \mathbb{R}^{k \times k}$ and $B \in \mathbb{R}^{k \times p}$ are linear predictors computed from observed trajectory data. To obtain such an

approximation from data, we gather data in the form of snapshot matrices

$$X = \begin{bmatrix} x_1 & , & \cdots & , & x_m \end{bmatrix} \tag{13}$$

$$Y = \begin{bmatrix} y_1 & , & \cdots & , & y_m \end{bmatrix} \tag{14}$$

$$U = \begin{bmatrix} u_1 & , & \cdots & , & u_m \end{bmatrix} \tag{15}$$

as before, where we now have m state observations with $y_i = F_u(x_i, u_i)$ for $i = 1, \ldots, m$. We then lift the X and Y data as in Eqs. 7 and 8 and perform the minimization

$$\min_{A,B} \|\Psi_Y - A\Psi_X - BU\|_2^2 \tag{16}$$

or as a least squares problem,

$$\min_{M} \|V - MW\|_2^2 \tag{17}$$

where

$$W = \begin{bmatrix} \Psi_X \\ U \end{bmatrix} \begin{bmatrix} \Psi_X \\ U \end{bmatrix}^\intercal \quad , \quad V = \Psi_Y \begin{bmatrix} \Psi_X \\ U \end{bmatrix}^\intercal ,$$

A is given by the first k columns of M, and B is given by the final p columns of $M \in \mathbb{R}^{k \times (k+p)}$.

IV. Results

A. Data collection

In order to apply the Koopman MPC framework to the foil stabilization problem, we begin by gathering trajectory data by simulating the model described in Sec. II of the pinned foil in an unsteady free stream flow. The panel method simulations are computed with a first-order Euler timestep of 0.02s. Each of these steps takes an average of 1.41s to compute, largely due to the interactions between the 200 point vortices, as well as their interactions with the 100 surface panels. Measurement data are collected every 0.06s. For the operator calculation, data is gathered from a single trajectory of 100s (1,666 total measurements). In this simulation, the rotor torque is chosen from a standard normal distribution, $\mathcal{N}(0, 1)$ every 0.06s, and held constant over 0.06s (3 simulation timesteps). The free stream flow specified here is given by

$$u = U_0(t)\Big(\cos(\phi(t)), \sin(\phi(t))\Big) \tag{18}$$

$$U_0(t) = 1 + 0.2\sin(t/\pi) + \epsilon_1 \tag{19}$$

$$\phi(t) = \frac{\pi}{6}\sin(t) + \frac{\pi}{12}\sin(2.5t) + \frac{\pi}{15}\sin(0.4t) + \epsilon_2 \tag{20}$$

where $\epsilon_1 \sim \mathcal{N}(0, 1/60)$ and $\epsilon_2 \sim \mathcal{N}(0, \pi/108)$ are noise terms.

For all simulations included here, the inertias of the foil and the rotor are taken to be equal; the fluid density and body length are both scaled to unity.

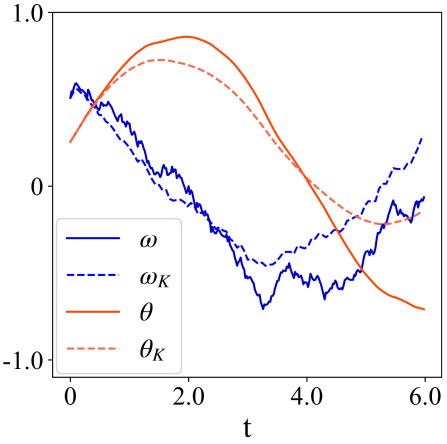

Fig. 3: The values of θ and ω measured in simulation (solid), compared with their estimates θ_K and ω_K (dashed) which are projected from the same initial states using iterative multiplication by the Koopman operator for a sequence of forcing torques τ drawn from a normal distribution of zero mean and unit variance.

B. Lifting and Operator Computation

Once the trajectory data is generated by running the simulations as described in Sec. IV-A, this data is stored in snapshot matrices as in Eqs. 13-15. The stored states are the foil angle and angular velocity, as well as two pressure measurements p_a, p_b on the foil body at the locations shown in Fig. 1. That is, the measurement vector is

$$x = [\theta, \omega, p_a, p_b]^\intercal. \tag{21}$$

To carry out the lifting of these states, as in Eq. 7-8, the dictionary functions are chosen to be all monomials in the measured states of up to order 3, as well as the state itself.

With the lifted states, the operators A and B are computed by solving the least squares problem in Eq. 17. This is computed as $M = VW^\dagger$ where $\dagger$ represents the Moore-Penrose pseudoinverse.

To assess how well the approximated Koopman operator representation of the system captures the nonlinear fluid robot interactions we compare the prediction of the operator to a full panel method simulation. Fig. 3 shows the trajectories of θ and ω for the foil placed in the flow as described above along with the predictions given by the propagating the lifted initial condition with the approximated Koopman operator. The torque τ chosen here is chosen from a normal distribution $\tau \sim \mathcal{N}(0, 1)$ on each step, as was done in the training data used for computing the approximate Koopman operator. While not perfect, this figure indicates that the linear operator gives sufficient predictive capability to be implemented in a predictive control framework.

We also note here that the Koopman based computation of the A and B predictor matrices is based on the assumption that the data is obtained from an underlying time-invariant control system of the form of Eq. 11. However, the numerical simulation of the hydrofoil does include explicit time-dependence, as the free stream flow magnitude and angle

vary in time. Essentially, applying the EDMD computation as described in Sec. III-B to this system amounts to obtaining a best-fit linear time invariant (LTI) system in the lifted space. The following references [33]–[35] discuss extensions of DMD, EDMD, and Koopman-based methods to nonautonomous systems. Most of these methods involve considering multiple time scales or a sliding window approach to DMD or EDMD, which allows the matrices A and B to be updated from new data online. In what follows, we show that the LTI approximation in lifted space captures the nonlinearities of the system sufficiently to be applied for control without accounting for the time dependence.

C. MPC Implementation

With the operators A and B computed, we now develop an MPC formulation to stabilize the foil angle to zero while not exceeding actuator constraints. For this, we use the following cost function at each timestep, denoted by j,

$$J_j = \begin{bmatrix} \theta_j \\ \omega_j \\ \Omega_j \end{bmatrix}^\intercal \begin{bmatrix} q_\theta & 0 & 0 \\ 0 & q_\omega & 0 \\ 0 & 0 & q_\Omega \end{bmatrix} \begin{bmatrix} \theta_j \\ \omega_j \\ \Omega_j \end{bmatrix} + r\tau_j^2 \tag{22}$$

so that the angular displacement and angular velocity of the foil θ and ω are penalized, as well as the control effort τ and the magnitude of the rotor velocity Ω. The values of the weights chosen here are $q_\theta = q_\omega = 5$, $q_\Omega = 0.1$, and $r = 0.01$. This is implemented with a control timestep of 0.06s and a horizon length of $N = 40$ steps (2.4s). With this, the MPC control is computed on each timestep by solving the quadratic program

$$\min_{u_t,\ldots,u_{(t+N-1)}} \sum_{j=t}^{t+N-1} J_j \tag{23a}$$

$$\text{subject to:} \quad \Psi(x_{j+1}) = A\Psi(x_j) + B\tau_j \tag{23b}$$

$$\Omega_{j+1} = \Omega_j - \Delta t \tau_j / I_r \tag{23c}$$

$$-\Omega_{\text{max}} \leq \Omega_j \leq \Omega_{\text{max}} \tag{23d}$$

$$-\tau_{\text{max}} \leq \tau_j \leq \tau_{\text{max}} \tag{23e}$$

$$\text{for} \quad j = t, \ldots, t+N-1$$

where the cost is given in Eq. 22 and the states θ_j and ω_j are included within the lifted state $\Psi(x_j)$. The two actuator constraints considered are to not exceed the maximum torque (23e) that can delivered by the motor driving the reaction wheel or the maximum spin rate (23d) that the motor can attain. In order to enforce the constraint on $\Omega = -\frac{1}{I_r}\int_0^t \tau dt$, this spin rate is simply tracked as an additional state, with updates performed via first order timestep, as in Eq. 23c. So, on each timestep t, the current measurement x_t given by Eq. 21 is lifted to $\Psi(x_t)$ and the optimization problem 23 is solved for $u_t, \ldots, u_{(t+N-1)}$, using the Koopman approximation matrices A and B to propagate the lifted state over the horizon. Then, the first input of this sequence, u_t is applied to the system. This optimization takes 0.043s on average, which is shorter than the control timestep, enabling real-time control.

D. Results

In Fig. 4 we show the results of the Koopman MPC applied on the nonlinear system model described in Sec. II for stabilizing the foil. The torque constraint is set to $\tau_{\text{max}} = 0.5$ and the rotor angular velocity constrain is set to $\Omega_{\text{max}} = 1.0$ for this case. Fig. 4a shows the magnitude of the free stream

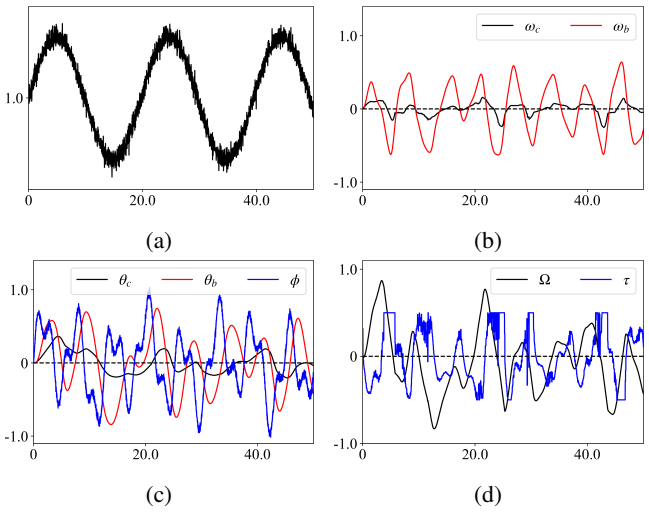

Fig. 4: (a) Variation in the free stream velocity magnitude, U_0 over time. (b) Foil angular velocity with zero control input ω_b, with τ from MPC ω_c. (c) Foil angle, θ_b, with zero control input (red), θ_c (black) when the control input is τ from MPC, and the free stream flow angle ϕ. (d) Rotor angular velocity Ω and torque τ commanded by the Koopman MPC.

fluid velocity, which is given by Eq. 19. The free stream fluid angle, given by Eq. 20 is shown in Fig. 4c. Fig. 4c compares the foil angle from a simulation with the Koopman MPC to an uncontrolled simulation and Fig. 4b shows the same comparison for the foil angular velocities. We see that the controlled foil angle θ_c performs much smaller oscillations than an uncontrolled foil angle θ_b, with an RMS value of $\theta_c^{\text{RMS}} = 0.145$ and $\theta_b^{\text{RMS}} = 0.410$ radians. The controlled foil angular velocity ω_c is on average much smaller in magnitude than the angular velocity ω_b of the uncontrolled foil, with $\omega_c^{\text{RMS}} = 0.079$ and $\omega_b^{\text{RMS}} = 0.35$. Fig. 4d shows the rotor torque actuation commanded by the MPC for the controlled simulation, along with the rotor angular velocity Ω. In places the torque appears like an inverted image of the flow angle ϕ, even though this angle is not provided to the controller, implying that the Koopman operator is encoding the state of the fluid through the two surface pressure measurements. The rotor velocity Ω does not saturate the constraint for these flow conditions, however the torque τ does reach its limit.

In order to illustrate the effect of the spin rate constraint on the performance we show an additional simulation in which the Ω constraint is active during the simulation. Results from a simulation in the same flow with Ω_{max} set to 0.7 and other parameters maintaining the same value are shown in Fig. 5. In this case, we see that Ω is extended to its limit, though only briefly, and the performance in terms of foil stabilization

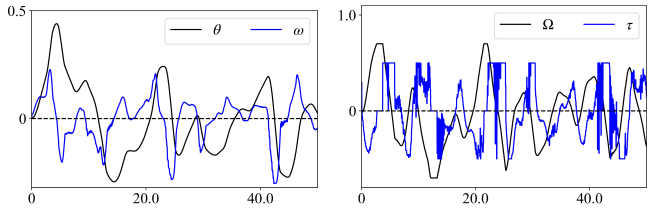

(a) (b)

Fig. 5: (a) Foil angle and angular velocity and (b) rotor angular velocity and torque for a smaller rotor speed limit $\Omega_{\max} = 0.7$.

suffers somewhat in comparison to the previous case, though the MPC does show stabilizing effects in comparison to the uncontrolled system, as for this case we have $\theta_c^{\text{RMS}} = 0.171$ and $\omega_c^{\text{RMS}} = 0.102$.

V. Conclusion

We have demonstrated the effectiveness of a Koopman operator based model predictive control scheme for the application of stabilizing a pitching hydrofoil in an unsteady free stream flow. This work could potentially be extended to develop data driven control methods for a swimming robot in an unsteady flow, which remains a significant challenge for underwater autonomous exploration. These methods could also be extended to give such a robot enhanced adaptability, by updating the operator online to account for changing flow characteristics or including preview information about the flow obtained from other distributed robots or sensors.

References

[1] M. S. Triantafyllou, G. D. Weymouth, and J. Miao, "Biomimetic survival hydrodynamics and flow sensing," *Annual Review of Fluid Mechanics*, vol. 48, no. 1, 2016.

[2] M. S. Triantafyllou and G. Triantafyllou, "An efficient swimming machine." *Scientific American*, vol. 272, no. 3, p. 64, 1995.

[3] J. W. Roberts, "Control of underactuated fluid-body systems with real-time particle image velocimetry," Ph.D. dissertation, 2012.

[4] C. W. Rowley, I. Mezić, S. Bagheri, P. Schlatter, and D. S. Henningson, "Spectral analysis of nonlinear flows," *Journal of Fluid Mechanics*, vol. 641, pp. 115–127, 2009.

[5] P. J. Schmid, "Dynamic mode decomposition of numerical and experimental data," *Journal of fluid mechanics*, vol. 656, pp. 5–28, 2010.

[6] M. Korda and I. Mezic, "Linear predictors for nonlinear dynamical systems: Koopman operator meets model predictive control," *Automatica*, pp. 149–160, 2018.

[7] E. Kaiser, J. N. Kutz, and S. L. Brunton, "Data-driven discovery of Koopman eigenfunctions for control," 2017. [Online]. Available: https://arxiv.org/abs/1707.01146

[8] S. E. Otto and C. W. Rowley, "Koopman operators for estimation and control of dynamical systems," *Annual Review of Control, Robotics, and Autonomous Systems*, vol. 4, pp. 59–87, 2021.

[9] Y. Han, W. Hao, and U. Vaidya, "Deep learning of Koopman representation for control," in *Proceedings of the Control and Decision Conference*. IEEE, 2020, pp. 1890–1895.

[10] D. Bruder, X. Fu, R. B. Gillespie, C. D. Remy, and R. Vasudevan, "Data-driven control of soft robots using Koopman operator theory," *IEEE Transactions on Robotics*, vol. 37, no. 3, pp. 948–961, 2021.

[11] G. Mamakoukas, M. L. Castaño, X. Tan, and T. D. Murphey, "Derivative-based Koopman operators for real-time control of robotic systems," *IEEE Transactions on Robotics*, vol. 37, no. 6, pp. 2173 – 2192, 2021.

[12] B. Pollard and P. Tallapragada, "An aquatic robot propelled by an internal rotor," *IEEE/ASME Transaction on Mechatronics*, vol. 22, no. 2, pp. 931–939, 2017.

[13] B. A. Free, J. Lee, and D. A. Paley, "Bioinspired pursuit with a swimming robot using feedback control of an internal rotor," *Bioinspiration and Biomimetics*, vol. 15, no. 3, p. 035005, 2020.

[14] B. Pollard and P. Tallapragada, "Passive appendages improve the maneuverability of fish-like robots," *IEEE/ASME Transactions on Mechatronics*, vol. 24, no. 4, pp. 1586–1596, 2019.

[15] B. Pollard, V. Fedonyuk, and P. Tallapragada, "Swimming on limit cycles with nonholonomic constraints," *Nonlinear Dynamics*, vol. 97, no. 4, p. 2453 – 2468, 2019.

[16] J. Lee, B. Free, S. Santana, and D. A. Paley, "State-feedback control of an internal rotor for propelling and steering a flexible fish-inspired underwater vehicle," in *Proceedings of the American Control Conference*. IEEE, 2019, pp. 2011–2016.

[17] B. L. Stevens, F. L. Lewis, and E. N. Johnson, *Aircraft control and simulation: dynamics, controls design, and autonomous systems*. John Wiley & Sons, 2015.

[18] S. TIFFANY and M. Karpel, "Aeroservoelastic modeling and applications using minimum-state approximations of the unsteady aerodynamics," in *30th Structures, Structural Dynamics and Materials Conference*, 1989, p. 1188.

[19] M. Goman and A. Khrabrov, "State-space representation of aerodynamic characteristics of an aircraft at high angles of attack," *Journal of Aircraft*, vol. 31, no. 5, pp. 1109–1115, 1994.

[20] M. Bhatia, M. Patil, C. Woolsey, B. Stanford, and P. Beran, "Stabilization of flapping-wing micro-air vehicles in gust environments," *Journal of Guidance, Control, and Dynamics*, vol. 37, no. 2, p. 592–607, 2014.

[21] G. Sedky, A. R. Jones, and F. Lagor, "Lift regulation during transverse gust encounters using a modified Goman Khrabrov model," *AIAA Journal*, vol. 58, no. 9, pp. 3788–398, 2020.

[22] J. M. Lidard, D. Goswami, D. Snyder, G. Sedky, A. R. Jones, and D. A. Paley, "Output feedback control for lift maximization of a pitching airfoil," *Journal of Guidance, Control, and Dynamics*, vol. 44, no. 3, pp. 587–594, 2021.

[23] A. Lasota and M. C. Mackey, *Chaos, Fractals, and Noise : Stochastic Aspects of Dynamics*. Springer, 1994.

[24] M. Budisic, R. Mohr, and I. Mezić, "Applied Koopmanism," *Chaos: An Interdisciplinary Journal of Nonlinear Science*, vol. 22, p. 047510, 2012.

[25] S. Klus, P. Koltai, and C. Schütte, "On the numerical approximation of the Perron-Frobenius and Koopman operator," *arXiv preprint arXiv:1512.05997*, 2015.

[26] H. C. et.al, "On the use of simulation in robotics: Opportunities, challenges, and suggestions for moving forward," *Proceedings of the National Academy of Sciences*, vol. 118, no. 1, 2020.

[27] J. Katz and A. Plotkin, *Low-Speed Aerodynamics*. Cambridge University Press, 2001.

[28] L. L. Erickson, "Panel Methods - An Introduction," *NASA Technical Paper*, 1990.

[29] S. Peitz, S. E. Otto, and C. W. Rowley, "Data-driven model predictive control using interpolated koopman generators," *SIAM Journal on Applied Dynamical Systems*, vol. 19, no. 3, pp. 2162–2193, 2020.

[30] C. Folkestad and J. W. Burdick, "Koopman NMPC: Koopman-based learning and nonlinear model predictive control of control-affine systems," in *2021 IEEE International Conference on Robotics and Automation (ICRA)*, 2021, pp. 7350–7356.

[31] M. O. Williams, I. G. Kevrekidis, and C. W. Rowley, "A data–driven approximation of the Koopman operator: Extending dynamic mode decomposition," *Journal of Nonlinear Science*, vol. 25, no. 6, pp. 1307–1346, 2015.

[32] S. Klus, F. Nüske, S. Peitz, J.-H. Niemann, C. Clementi, and C. Schütte, "Data-driven approximation of the Koopman generator: Model reduction, system identification, and control," *Physica D: Nonlinear Phenomena*, vol. 406, p. 132416, 2020.

[33] S. Macesic, N. Crnjaric-Zic, and I. Mezic, "Koopman operator family spectrum for nonautonomous systems," *SIAM Journal on Applied Dynamical Systems*, vol. 17, no. 4, pp. 2478–2515, 2018.

[34] H. Zhang, C. W. Rowley, E. A. Deem, and L. N. Cattafesta, "Online dynamic mode decomposition for time-varying systems," *SIAM Journal on Applied Dynamical Systems*, vol. 18, no. 3, pp. 1586–1609, 2019.

[35] S. L. Brunton, M. Budišić, E. Kaiser, and J. N. Kutz, "Modern koopman theory for dynamical systems," *arXiv preprint arXiv:2102.12086*, 2021.